

For Heavy Biomolecules, Simulations of a Digital Ion Filter and A Digital Ion Trap

Mahesh Tubaki

Electronics and Communication Engg
Govt Polytechnic - Belagavi

Satheesha K M

Electronics and Communication Engg
KPT - Mangalore

ABSTRACT

WDFs are wave digital filters that are modelled after classical filters, usually in lattice or ladder topologies or extensions of such designs. They offer excellent qualities in terms of coefficient precision, dynamic range, and, most importantly, stability under finite-arithmetic circumstances. A thorough examination of WDF theory is provided. Several objectives are set for this book: to provide an introduction to those who are unfamiliar with the subject, to emphasize practical aspects as a guide for those who want to design or apply WDFs, and to provide insight into the broad range of aspects of WDF theory and its many relationships with other fields, particularly in the signal-processing field. As a result, mathematical analyses are only presented if they are required for acquiring critical insight, and all specifics of a more unique character are referred to current literature.

Keywords: WDF, Circuits, System, Filters, Digital Filters, Blocks

Date of Submission: 02-03-2022

Date of Acceptance: 16-03-2022

I. INTRODUCTION

The significance of digital filters has long been recognized. Digital filters are widely used in a number of applications, and there is a great quantity of literature on the subject, including numerous publications in several languages. A recent instructional paper on the general topic of digital filtering, published in the Centennial Issue of the IEEE TRANSACTIONS ON CIRCUITS AND SYSTEMS [1], is available to interested readers.

Wave digital filters (WDFs) are a family of digital filters that, in addition to no recursive digital filters and digital filters composed of simple first- and second-order sections in cascade, are of special interest. They were initially described publicly in 1970 [2], [3], and a first thorough study was published in 1971 [4] (a shortened version is [5], while [6] provides a few more results). Several early articles on the subject [4], [7]- [9], as well as several additional publications with a connection to our subject [10]-[13], are reproduced in [10]. A variety of books [14]-[28] are now available that provide some basic information. The goal of this study is to provide a high-level review of the current state of the art in the field of WDFs.

WDFs are a type of digital filter that is connected to classical filter networks (see, for example, [10]), and are preferably lossless filters placed between resistive terminations. As a result, every

WDF has a reference filter from which it is generated. The underlying explanation for the numerous intriguing aspects of WDFs, as well as the slightly more difficult access to theory and design of these digital filters, is this connection. Indeed, while translating a given reference filter into a WDF is rather simple, choosing an appropriate reference structure and designing it needs some acquaintance with classical filter theory, including features of microwave filter theory. The similarity between a WDF and its reference filter is based on the usage of so-called wave qualities known from classical circuits as signal parameters [32], which is how the name for the class of digital filters discussed in this study came about. For the sake of clarity, Kirchhoff circuits are circuits whose topological restrictions are the Kirchhoff equations (classical circuits and their multidimensional extensions).

There isn't just one type of WDF, but a plethora of subclasses, each of which can be further subdivided into multiple families, etc. This represents the diversity of structures accessible in traditional circuits, and the designer should choose the reference filter structure that leads to the best overall solution for the issue at hand. Fortunately, several simple forms of WDFs exist that are adequate to suit most typical requirements for filter performance, structural simplicity and adaptability, and so on, while requiring only a basic understanding of classical circuits to construct.

Wave digital filtering is a notion that may be applied to any number of dimensions. All-important qualities that hold in the one-dimensional situation are conserved in this instance, regardless of degree or number of dimensions. This includes low requirements for coefficient word lengths, good dynamic range, the absence of parasitic oscillations (i.e., nonperiodic oscillations such as those that may occur in a multidimensional digital filter because such circuits are not finite-state machines), forced-response stability, and so on. Once a proper multidimensional reference filter is known, computing the WDF is once again simple. The latter, on the other hand, is now the most difficult to determine. Important answers to this challenge have already been found, and more work on this topic is now underway [45].

We shall only be working with constant and multirate WDFs in this study. WDFs are also good candidates for adjustable and adaptive filtering due to their strong stability qualities. It's not unexpected, therefore, that they're closely connected to the most common forms of adaptive digital filters [a], although this is a topic that can only be briefly discussed. One-dimensional circuits will be the exclusive focus of Sections II through X. Section XI considers extensions to the multidimensional case. As a general guideline, we'll focus on key ideas and aspects that are crucial to the designer right now. We will consult the current literature for more sophisticated theoretical analysis.

**BASIC PRINCIPAL
 Realizability**

A series of difference equations completely describes a digital filter mathematically. The arithmetic operations defined by these equations must be ordered sequentially, say, within a time interval of duration T, and they must repeat regularly at a rate, in order to create a digital filter.

$$F = 1/T \quad (1)$$

The realizability conditions [4], and the former alone as computability condition [70], are the precedence and periodicity requirements.

A signal-flow diagram is a framework that may be used to illustrate the mathematical description of a digital filter. Depending on whether the aforementioned realizability requirements are met or not, the latter might be labelled as realisable or unrealizable. The testing of realizability is quite simple for the most often encountered digital filter topologies. However, a more exact theorem is required for more generic structures.

Some more vocabulary is necessary in order to articulate this. First, keep in mind that the delays in a digital filter network don't have to be multiples of T; they might be fractions of T, as is already the

case when considering the time necessary to do the requisite arithmetic operations. We call a circuit full-synchronic if all delays are multiples of T; otherwise, half-synchronic if the periodicity criterion is met. A digital filter's signal-flow diagram is said to be correct if it is linked and does not contain any branches with a zero transfer function.

If each of the loop's branches has the same orientation with respect to a particular loop orientation, the loop is said to be directed. The sum of the delays in the branches oriented in the same direction as the loop minus the sum of the delays in the branches oriented oppositely to the loop is the overall delay of a particular loop (with regard to a given orientation). While negative delays are interesting for some theoretical studies, this is clearly not the case for real circuits. As a result, unless otherwise specified, we will always presume that there are no unfavorable delays. If there are no delay elements in a branch, route, or loop, it is termed delay free.

Theorem 1 : If and only if the following requirements are met, the signal-flow diagram of a suitable digital filter can be realised at a rate of $F = 1/T$:

- It doesn't have any directed loops that aren't delayed.
- Any loop's total delay (directed or undirected) is a multiple (zero, positive, or negative) of T.

Clearly, the second criterion is met fundamentally by a full-synchronic digital filter. The necessity of both criteria is obvious. Indeed, if a delay-free directed loop exists, such as the one shown in Fig. 1(a) (which consists of two adders and a multiplier of coefficient y), it is impossible to create a sequence in which the arithmetic operations required by this loop may be performed. If there is a delay, such as $T_1 + T_2$, in the loop of Fig. 1(b), it must be a multiple of T, since otherwise the filter would not be able to function at the rate F.

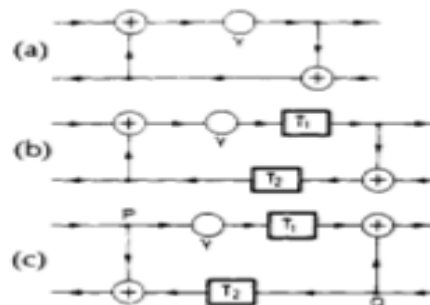


Fig No. 1: A directed loop with no delay. (b) A directed loop with T and T2 delays. (c) A loop with delays J and T that is undirected.

BUILDING BLOCKS

To get to the structures we want, we need to look at how elements and sources are translated from the reference domain to the WDF domain (and vice versa). We'll look at single-port, two-port, and multiport components first. Because the equivalence can only hold in the \$-domain, as mentioned at the start of Section 11-A, we always start with steady-state expressions. The steady-state equations explain a capacitance and an inductance (Table 1, first two columns) in the reference domain (cf. second row in Table 1)

$$V = R1/\psi \quad (2)$$

Indeed, V must be proportional to I and, since \$ is adopting the role of a complex frequency, proportionate to I/\$ and \$, respectively, because \$ is assuming the function of a complex frequency. The proportionality constant that determines the element's size can always be put in the numerator, in which case it has the resistance dimension.

Now we'll choose the same R value for the port resistance that we did in the previous step (16). (16) is obtained by combining (2) and (6).

$$Z = B^{-1}A \quad (3)$$

The resistance, the short circuit, the open circuit, the resistive source, and (albeit of lower relevance) the (pure) voltage source may all be approached in the same way. Table 1 also has the related findings, with the formula for the source voltage being $e = e(t,.) = EeP^m$, where E is a complex constant. The port resistance for the open circuit, short circuit, and voltage source (fourth, fifth, and last columns in Table 1) may be selected arbitrarily because the defining equations for these three situations do not contain any resistive parameter.

Capacitance	Inductance	Resistance	Short-circuit	Open-circuit	Resistive source	Voltage source
$V = IR/\psi$	$V = \psi RI$	$V = RI$	$V = 0$	$I = 0$	$V = E + RI$	$V = E$
$B = z^{-1}A$	$B = z^{-2}A$	$B = 0$	$B = -A$	$B = A$	$B = E$	$B = 2E - A$
$b(t_0) = a(t_0 - T)$	$b(t_0) = -a(t_0 - T)$	$b = 0$	$b = -a$	$b = a$	$b = e$	$b = 2e - a$

Fig No. 3 : Digital Ions Filter

Supercapacitances and super inductances are further one-port components that can be defined [89], but they will not be explored in this study because they have not been proven to provide genuine benefits. Selecting a port resistance equal to

R for a current source with source current E/R is equivalent to substituting 6 and b in the last column of Table 1 with - 6 and - b, respectively.

It's worth noting that the constant to may vary depending on the signal in question. This is owing to the presence of delays (perhaps also fractional delays, though they are not included in Table 1), which must be properly considered if the relative time at various points in the circuit is to be properly taken into account. Consider the statement (18a), which may alternatively be written as $b(t,.) = a(t,.)$, with t being supplied by (19) and t!,, b.

$$t_m = t_0 + mt_m$$

$t; = t_0 - T$ and $t; = t, - T$ are examples of this. Clearly, they yields the same sequence of time instants as t, but this need not be the case if the delay is not a multiple of T, as will be the case in the following sections.

The gyrator, as seen in the third column of Table 2, is a fairly simple element to implement. Several realisations of the ideal transformer are of interest. Table 3's first column contains one of these, and the others will be explained later. It is important to note that the port resistances at the two ports, R and R,, do not have to be equal; so, (16) must be changed by

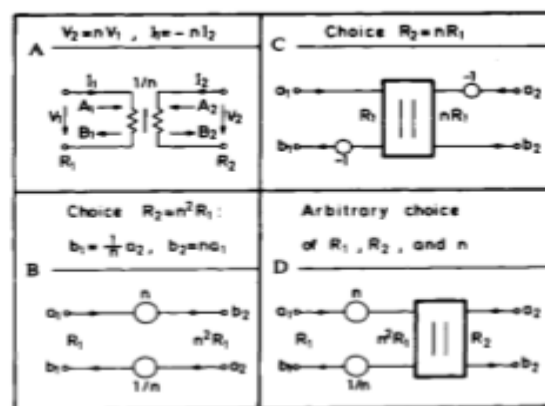


Fig No. 3 : Ideal Transformer

The module should be able to handle and separate ions with a mass resolving power R on the order of a hundred thomson. Furthermore, the radial phase space of the outgoing ion bunch must be small enough to permit a sequence of 2-mm holes downstream. Its temporal breadth must be smaller than 100 milliseconds in order to facilitate time-of-flight conformation separation at the ion mobility cell and a high-density ion bunch in the X-ray beam's interaction zone. Two constraints must be followed in order to preserve the native structure of the proteins: The ions' kinetic energy should be less than a few hundred eV, and the background gas pressure should be less than 102 hPa.

IONS AND DIGITAL RF FIELD

Despite the fact that the fundamental concepts and concerns date back to 1973 [14,15], the digital (square-wave) functioning of quadrupole ion filters and traps did not become widely used until the early twenty-first century [16e21]. In the meanwhile, it has established itself as a reliable technique.



Fig No.4 : The MS SPIDOC prototype's main modules. The module discussed in this paper is highlighted in red.

a non-sinusoidal alternative to sinusoidal devices. Within the span of one experimental cycle, the digital technique allows the system's mass range to be changed from single atoms to viruses. The frequency may be altered remotely without interrupting the measurement because high-frequency switches are used instead of resonant circuits. This considerably enhances a system's versatility, pushing the usage of the digital method in an increasing number of applications [22e24]. The upper V_H and lower V_L voltages, as well as the duty cycle d , define a square-shaped waveform (see Fig. 2) [25]: The RF waveform's amplitude is defined as

$$V_a = \frac{V_h - V_l}{2}$$

Two neighboring quadrupole rods' potentials alternate between V_H and V_L . The duty cycle is described as follows:

$$d = \frac{T_h}{T}$$

where T denotes the entire period and t_H is the portion of the period during which V_H is used. At V_{off} a common offset voltage can be applied in relation to the ground potential.

$$V_{off} = \frac{V_h - V_l}{2}$$

The solutions of the Hill equation [26] explain the track of a charged particle inside an RF field. A numerical solution may be discovered for any sort of periodic RF field using cascading matrix multiplication, as proved by Kononov et al. [12] and Brabeck et al. [13] for quadrupole ion guides operating with a square-shaped waveform. The trajectory of an ion with mass m and charge Q is stable or unstable depending on the stability factors a and q .

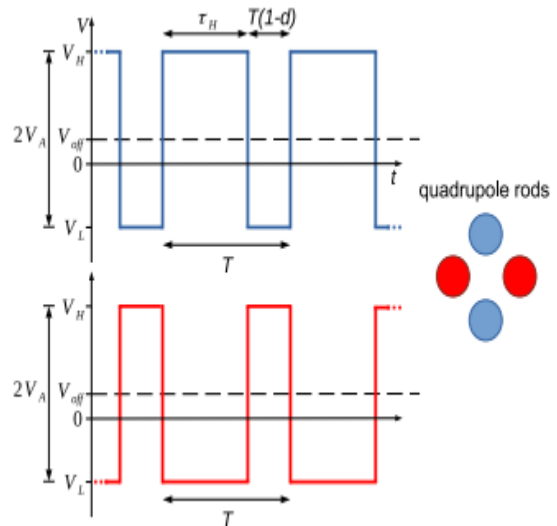


Fig No.5 : 2. Duty cycle d , amplitude V_A , period T , offset voltage V_{off} , square-shaped (digital) waveform for quadrupole device operation with high V_H and low voltage V_L , duty cycle d , amplitude V_A , period T , offset voltage V_{off} .

Stability diagrams (see Fig. 3(a)) may be used to depict the (a, q) parameter-space areas of stable and unstable ion trajectories. For various duty cycles, the areas may be computed using the matrix approach [12,13]. These stability diagrams may also be represented in coordinates of duty cycle d and frequency f for ions with certain mass-to-charge m/z values, where z is the charge state, given immediately available experimental data. The frequency for each q may be calculated using Equation (4). This is illustrated in Fig. 3(b) for the case of a 14^+0 (no extra DC-voltage component U) for the boundaries of the stability zone depicted in Fig. 3(a) as a function of duty cycle.

EXPERIMENTAL SETUP

An entry-side hexapole, a quadrupole-filter assembly consisting of a quadrupole pre-guide, filter, and post-guide, an encapsulated linear quadrupole ion-trap with two sets of four pins each, and an exit-side hexapole make up the current module (Fig. 4). It's worth noting that ion filtering and accumulation have been described in single digitally-driven linear quadrupole devices [24,28,29]. However, we chose distinct filtering and accumulation/storage components, which allows for independent optimization of these components and increases the overall flexibility of the MS SPIDOC system. Should equivalent scientific circumstances be observed in future tests, the ion mobility element, for example, may be put between the mass filter and the trap.

Ion selection is usually accomplished with a (digital) ion trap by altering the stability conditions for the trapped particles, i.e. by scanning the trap-frequency. Ion selection and trapping/bunching are separated in this system to allow for the use of various devices for distinct functions. This eliminates space-charge effects when filtering a fully loaded trap [32e34] and aids analysis in the event of collision-induced dissociation during trapping and ejection processes.

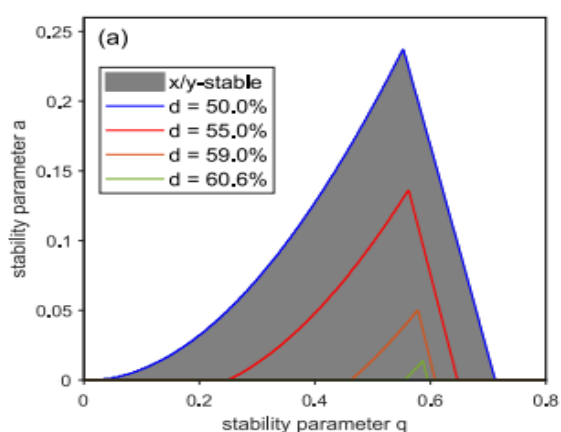


Fig No. 6 : Stability diagram for a digital quadrupole ion guide derived using the matrix approach in the (a, q) parameter space for various duty cycles.

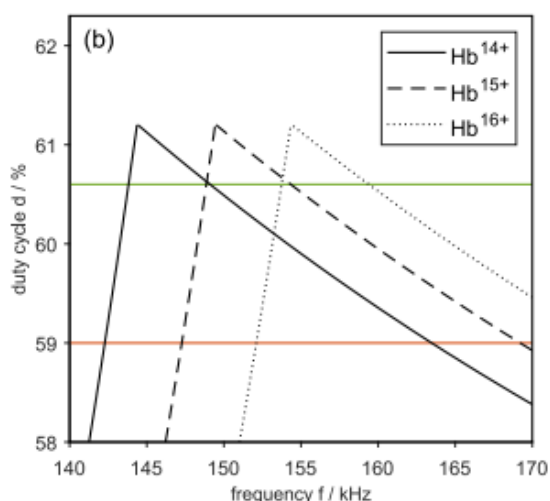


Fig No. 7 : Stability Diagram Parameter

The ion optics simulation tool SIMION [35], version 8.1 [36], is used to calculate the electric fields and ion trajectories on a grid mesh with a spatial resolution of 0.2 mm/gu (gu-"grid unit"). SIMION is a commonly used software for calculating ion trajectories in electric fields. It has a lot of features and may be extended with third-party extensions. The computation time steps of the ion

trajectories have been kept to less than one tenth of the highest utilized RF frequency. Ions are treated as point-like particles with no intrinsic energy in SIMION. As a result, the thermalization behavior outlined in Sec. 4.3 solely applies to translational energies, ignoring energy transfers to internal degrees of freedom.

Simulations are carried out using ions with a mass of 64 452 u and a charge state of $z = 14-15$, which correspond to a non-covalent human haemoglobin holoprotein complex, with an average mass of 64 452 u determined by the amino acid sequences of its two alpha and two beta chains (Uniprot: P69905 residues 2e142 and P68871 residues 2e147, respectively) and the addition of four heme cofactor. The results will enable for quantitative comparisons with measurement data during the module's eventual experimental characterization. At the entry-side aperture, a set of 500 ions is begun with the start parameters indicated in (Table 1). The latter comes from simulations of the upstream module conducted by other project participants. To compensate for losses due to background-gas collisions, differences in offset potentials between two successive components of 1 V are employed to give ions with adequate axial kinetic energy.

Hexapoles

The hexapoles ("hexapole in" and "hexapole out" in Fig. 4) transport ions from the entry-side aperture ("aperture in," 2 mm diameter) into the filter area and from the trap region to the exit-side aperture ("aperture out," 2 mm diameter). The hexapoles had been established for the MS SPIDOC partners to ensure that the modules had the same ion transition. This assures the prototype's modularity.

According to the MS SPIDOC collaboration, these hexapoles have a rod diameter of 4 mm, a rod-axis distance of $r_0 = 14.4$ mm, and a length of 103 mm. Table 2 shows the digital RF voltage supplied to the hexapole rods. Despite the upstream ESI source, the pressure in the entry-side hexapole of 106 hPa is quite modest. This is because, as previously stated, the source is linked via an extra ion funnel and octupole guide, which improves differential pumping.

IONS TRANSMISSION WITHOUT TRAPPING

The kinetic energy of the ions is measured as they move through the module (Fig. 9) to guarantee that it never exceeds a few hundred eV, which is necessary for biomolecules (see introduction, Sec. 1). Filter settings for R 14 100 are used in the simulation depicted in Fig. 9, and trapping/ejection is deactivated. The axial kinetic

energy is shown by the blue lines, which rises or decreases depending on the offset potential illustrated in Fig. 4. Furthermore, due to the relatively high pressure in the trap zone (between roughly 330 and 370 mm), a continual drop in energy due to background-gas collisions is seen. The envelope of the standard deviation of the ions' total kinetic energy is shown in red. The ions have practically entirely axial kinetic energy where the red and blue lines intersect, i.e. outside of the filter zone. The transversal rf fields, on the other hand, increase their radial energy as they travel through the filter zone. The RFPotential settings determine the structure of the total kinetic energy, which in this case has three separate maxima at roughly 150, 210, and 270 mm. The maximum energy is attributable to the focusing potential given to the post-guide element, which is on the order of 420 eV and hence within the desired limit (Table 2).

CAPTURING AND THERMALIZATION BEHAVIOR

The pressure of the buffer gas is a vital parameter for the ion trap's operation, in addition to the accumulation mode's potential setup. The trapping efficiency η is defined as the ratio of the number of ions reaching the exit-side aperture after being stored for 5 ms to the number of ions entering the trap through the entry-side endcap to characterize the trap performance (Fig. 10). Because the ions have distinct phase spaces for different filter settings at the trap's entrance, the trapping effectiveness is partially dependent on the filter parameters. Most ions do not lose enough energy to be captured at $p = 3, 103 \text{ hPa}$ and escape the trap immediately after reflection at the exit-side potential through the entropy.

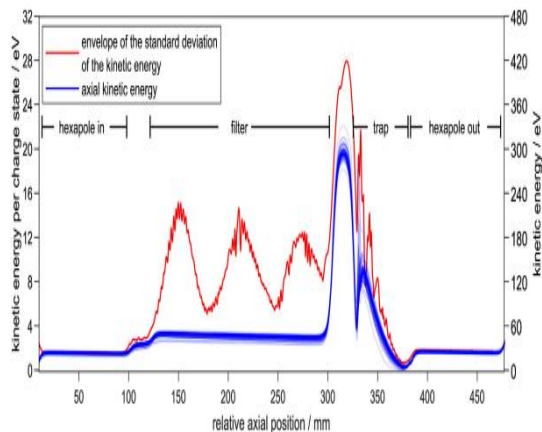


Fig No.8 : For filter settings of $f = 14 \text{ 150 kHz}$, $V_A = 14 \text{ 145 V}$, and $d = 14 \text{ 0.61}$, kinetic energy of Hb^{15} ions as a function of axial position when transmitted without trapping. A total of 100 ions' paths with various beginning points were

simulated. The axial energy components are shown by blue lines, whereas the radial energy components are represented by red lines.

In the following, we assume that the thermalization process causes the axial and transversal kinetic energy to equilibrate. Figure 11 depicts the loss of kinetic energy over time for a single ion as an example. The ion propagates between the endcaps at trapping periods of $t = 0.8 \text{ ms}$. An exponential energy loss is observed once the ion has lost enough energy to be trapped in the potential well of the pin electrodes ($t > 0.8 \text{ ms}$). There is a continual transfer of potential and kinetic energy due to the oscillating motion.

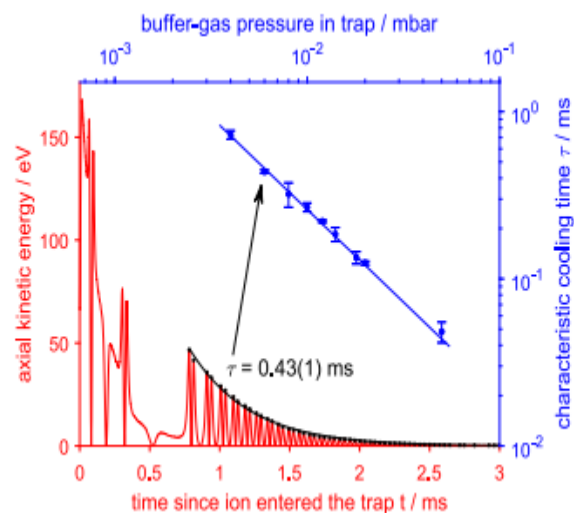


Fig No.9 : Example of an ion's axial kinetic energy over time following capture in the trap at $5, 103 \text{ hPa}$ (lower left half, red). To fit an exponential decline with thermalization time t , the maxima (black points) are employed. Characteristic cooling time as a function of buffer-gas pressure (upper right portion, blue). The arrow points to the data point derived from the red example. The line represents the data as a power-law fit.

An exponential energy loss is observed once the ion has lost enough energy to be trapped in the potential well of the pin electrodes ($t > 0.8 \text{ ms}$). There is a continual transfer of potential and kinetic energy due to the oscillating motion. However, the kinetic-energy peaks corresponding to the ion being in the middle of the potential well may be fitted with an exponential function $e^{-t/\tau}$ with a characteristic cooling time τ .

II. CONCLUSION

The simulations conducted in the current study under development for the MS SPIDOC apparatus at XFEL demonstrate that the provided

module is capable of filtering, accumulating, and thermalizing 4300 Th ions, such as Hb15, before releasing them as an ion bunch. The quadrupole filter's mass resolving power is around 100 for transmission efficiency close to 100%, and it may be enhanced to roughly 700 for transmissions on the order of 15%. A buffer-gas pressure of a few 102 hPa is adequate to collect and accumulate virtually all incoming ions in the digital ion trap. They can be expelled as a compacted lot with a smaller phase space than the entering ion cloud and an FWHM of the time-of-flight distributions on the order of a microsecond after thermalizing for a few milliseconds. As a result, the module meets the standards for biomolecule preparation. The ions' energy stays below 420 eV during the transmission. In addition, the buffer-gas pressure used to collect ions in the ion trap is within the desired range.

In future investigations, the parameter values of this module that are necessary to handle ions with orders of magnitude higher mass-to-charge ratios will be investigated. Additionally, the impacts of other buffer-gas species, as well as the usage of extra sets of pins, will be studied. Simultaneously, a prototype of this module will be created to check the functioning and practicability of all components in an experimental setting.

REFERENCE

- [1]. C. Uetrecht, K. Lorenzen, M. Kitzel, J. Heidemann, J.H. Robinson Spencer, H. Schlüter, J. Schulz, Native mass spectrometry provides sufficient ion flux for XFEL single-particle imaging, *J. Synchrotron Radiat.* 26 (3) (2019) 653e659, <https://doi.org/10.1107/S1600577519002686>
- [2]. M. Altarelli, The european x-ray free-electron laser facility in hamburg, proceedings of the 10th European Conference on Accelerators in Applied Research and Technology (ECAART10), *Nucl. Instrum. Methods Phys. Res. Sect. B Beam Interact. Mater. Atoms* 269 (24) (2011) 2845e2849, <https://doi.org/10.1016/j.nimb.2011.04.034>. URL, <http://www.sciencedirect.com/science/article/pii/S0168583X11003855>
- [3]. A. Kadek, K. Lorenzen, C. Uetrecht. In a flash of light: X-ray free electron lasers meet native mass spectrometry, *Drug Discov. Today Technol.* 10.1016/j.ddtec.2021.07.001, URL <https://www.sciencedirect.com/science/article/pii/S1740674921000172>
- [4]. M. Wilm, M. Mann, Analytical properties of the nano-electrospray ion source, *Anal. Chem.* 68 (1) (1996) 1e8, <https://doi.org/10.1021/ac9509519>, PMID: 8779426
- [5]. F. Lanucara, S.W. Holman, C.J. Gray, C.E. Eyers, The power of ion mobility-mass spectrometry for structural characterization and the study of conformational dynamics, *Nat. Chem.* 6 (4) (2014) 281e294, <https://doi.org/10.1038/nchem.1889>
- [6]. G.F. Brabeck, H. Koizumi, E. Koizumi, P.T.A. Reilly, Characterization of quadrupole mass filters operated with frequency-asymmetric and amplitude-asymmetric waveforms, *Int. J. Mass Spectrom.* 404 (2016) 8e13, <https://doi.org/10.1016/j.ijms.2016.04.002>. URL, <http://www.sciencedirect.com/science/article/pii/S1387380616300306>
- [7]. R. March, J. Todd. *Practical Aspects of Trapped Ion Mass Spectrometry, Volume IV: Theory and Instrumentation*, CRC Press, 2010. <https://books.google.de/books?id¼GLTftZ11eYC>
- [8]. J. Lee, M.A. Marino, H. Koizumi, P.T.A. Reilly, Simulation of duty cycle-based trapping and ejection of massive ions using linear digital quadrupoles: the enabling technology for high resolution time-of-flight mass spectrometry in the ultra high mass range, *Int. J. Mass Spectrom.* 304 (1) (2011) 36e40, <https://doi.org/10.1016/j.ijms.2011.03.011>. URL, <https://www.sciencedirect.com/science/article/pii/S1387380611001242>
- [9]. M. Sudakov, E. Nikolaev, Ion motion stability diagram for distorted square waveform trapping voltage, *Eur. J. Mass Spectrom.* 8 (3) (2002) 191e199, <https://doi.org/10.1255/ejms.491>.
- [10]. D. Wang, F.H.W. van Amerom, T. Evans-Nguyen, High-speed digital frequency scanning ion trap mass spectrometry, *Anal. Chem.* 85 (22) (2013) 10935e10940, <https://doi.org/10.1021/ac402403h>
- [11]. D. Manura, D. Dahl, *SIMION 8.0/8.1 User Manual: Covering SIMION Version 8.1.0.31*, Scientific Instrument Services, Incorporated, 2011. URL, <https://books.google.de/books?id¼bspWAQAACA>
- [12]. J. Zhang, G.R. Malmirchegini, R.T. Clubb, J.A. Loo, Native top-down mass spectrometry for the structural characterization of human hemoglobin, *Eur. J.*

- Mass Spectrom. 21 (3) (2015) 221e231, <https://doi.org/10.1255/ejms.1340>, arXiv:
- [13] Mass spectrometry for single particle imaging of dipole oriented protein complexes, Dec. 2022
- [14] S. Guan, A.G. Marshall, Equilibrium space charge distribution in a quadrupole ion trap, J. Am. Soc. Mass Spectrom. 5 (2) (1994) 64e71, [https://doi.org/10.1016/1044-0305\(94\)85038-0](https://doi.org/10.1016/1044-0305(94)85038-0)
- [15] Z.P. Gotlib, G.F. Brabeck, P.T.A. Reilly, Methodology and characterization of isolation and preconcentration in a gas-filled digital linear ion guide, Anal. Chem. 89 (7) (2017) 4287e4293, <https://doi.org/10.1021/acs.analchem.7b00356>